Article

Low-power detection of food preservatives by a novel nanowire-based sensor array

Dario Zappa [1,*]

[1] SENSOR Laboratory, DII, Università degli Studi di Brescia, Via Valotti 9, 25133 Brescia, Italy;
* Correspondence: dario.zappa@unibs.it; Tel.: +39-030-371-5767

Received: date; Accepted: date; Published: date

Abstract: Food preservatives are compound that are used for the treatment of food to improve the shelf life. In the food industry, is necessary to monitor all processes, for both safety and quality of the product. An electronic nose (or e-nose) is a biomimetic olfactory system that could find numerous industrial applications, including food quality control. Commercial electronic noses are based on sensor arrays composed by a combination of different sensors, which include conductometric metal oxide devices. Metal oxide nanowires are considered among the most promising materials for the fabrication of novel sensing devices, which can enhance the overall performances of e-noses in food applications. In the present work, is reported the fabrication of a novel sensor array based on SnO2, CuO and WO_3 nanowires deposited on top of commercial μHPs, provided by ams Sensor Solutions Germany GmbH. The array was tested for the discrimination of four typical compounds added to food products or used for their treatment to increase the shelf life: ethanol, acetone, nitrogen dioxide and ozone. Results are very promising: the sensors array was able to operate for long time consuming less than 50mW for each single sensor, and PCA analysis confirms that the device was able to discriminate between different compounds.

Keywords: Metal-oxides nanowires; chemical sensing; sensor array; electronic noses, food preservation;

1. Introduction

We all agree that nowadays we are living in the era of images, in which vision is considered the most important of the human senses. Nevertheless, sometime we forget that vision is only one of the five human senses (vision, hearing, olfaction, taste, and touch), and it cannot be always trusted alone. Our interaction with the surrounding environment, and even our own survival, depend on the combined information that we receive from all of them. Among these senses, olfaction is for sure the most mysterious and complex one, even if historically has been considered of a lower status in relation to the other senses [1]. Apparently, olfaction has lost in humans the importance that has in animals, as it is often involved during prey hunting and feeding [2]. However, it is one of our innate warning systems in case of danger, for example in case of fire. To give an idea on the importance of the olfactory systems, almost the 4% of the genomes of many higher eukaryotes is devoted to encode the proteins that are responsible of smell [3]. Olfaction is related also to cognition, as confirmed by many studies [4]: a particular smell can trigger a series of memories in people. Human beings possess an excellent ability to detect and discriminate odors, but they typically have great difficulty in identifying particular odorants.

Artificial olfaction (also called an electronic nose or e-nose) is a biomimetic olfactory system [5–7] that could find numerous industrial applications, such as indoor air & environmental monitoring [8–10], hazardous gas detection & customs security [11,12], medical care [13–15] and food quality control [16–18]. If we exclude the first prototype of a mechanical-based artificial olfaction system [19], the concept of an electronic nose was developed in 1964 by Wilkens and Hatman [20], and then taken up by Persaud in 1982 [21].

Preprints (www.preprints.org) | NOT PEER-REVIEWED | Posted: 13 May 2019 doi:10.20944/preprints201905.0138.v1

Peer-reviewed version available at Foods 2019, 8, 226; doi:10.3390/foods8060226

Among the large number of application of electronic noses, food quality and safety deserve a special mention. We can identify at least two main area in the food industry that benefit from the use of an artificial olfaction system. The first one is the detection of contaminants during food processing chains [22–24]. The preemptive assessment of the source of contaminants during all the steps required for food product preparation and handling is not always possible. Contaminating microorganisms may enter and reach the end-product through many parallel routes: though raw materials, air in the processing plant area, process surfaces, or even inadvertent personnel. Risk assessment tools like Hazard Analysis Critical Control Points (HACCP) are almost the standard approaches to detect processes prone to contamination risks [25–27]. However, built-in mechanisms on the food chain for in-process sampling and contamination screening are necessary, because would allow the food company to preventively stop the production, thus limiting the damage to just a part of the entire batch, without compromising it completely.

The second application of e-noses in the food industry is the quality control of raw materials and end-products, and in particular authenticity [28–30], food freshness [31], the presence of allergens and shelf life [32]. The increased demand for the long-term storage and preservation originate the need to develop methods that can easily track and assess food freshness. Moreover, authenticity of food is a rising issue in many countries, even market leaders. As an example, it is estimated that the rate of fraud of Parmigiano Reggiano cheese, a well-known Italian product, is between 20% and 40% worldwide, reaching a dramatic 95% in the United States [30,33].

Commercial electronic noses are based on sensor arrays composed by a combination of different sensors, which include conductometric [34][35], piezoelectric [36][37], field effect transistors [38], optical sensors [39] and many more [40], based on different materials and working principles. Among these, metal oxide (MOX) materials represent the current state of the art in the chemical sensing technology, and have been investigated largely due to their abundance, cheap and easy fabrication and high performances. In 1991, Yamazoe demonstrated that reducing the size of metal oxide materials to nanoscale could lead to a substantial enhancement of their sensing properties [41]. Therefore, the research focused on the development of these novel nanostructures, constantly improving the performances of the devices [42]. Among this novel generation of nanostructured materials, metal oxide nanowires are considered among the most promising for the fabrication of chemical sensing devices, due to their extremely high surface-to-volume ratio and their unique electrical and chemical properties [43–45]. These features allow quasi-1D structures like nanowires to outperform drastically their bulk counterparts.

As all other materials, however, metal oxides have some limitations that have inhibited an even larger diffusion as sensitive materials [46]. One of the critical requirements of these materials is that they are activated thermally, because chemical reactions that take place on their surface are promoted by temperature (usually 200-400°C). Therefore, a substantial part of the energy consumption of an electronic nose is related to its sensors heating. While this is not a big issue in food industries, where devices are always connected to the power line, it is a strong key factor limiting the design of portable equipment.

Thanks to the advances in the silicon semiconductor industry, there are now available on the market different micro-machined (MEMS) silicon micro hotplates (μHPs), which consist in a very thin membrane integrating both interdigited electrodes and a heating element able to reach more than 400°C with ease [47]. These substrates allow reducing drastically the energy consumption of a single sensor, moving from hundreds of mW to few tens during continuous operation, and are ideal candidates to be integrated into a portable e-nose. Moreover, due to the reduced thickness of the membrane, these hotplates exhibit a very small thermal inertia which enables the possibility of using smarter sampling techniques and further power saving operating modes, like fast temperature modulation and discontinuous operation [48–50]. Finally, the process steps required for the fabrication of these devices are compatible with the standard planar silicon technology. Therefore, it is possible to scale the fabrication to the mass production, breaking down the price of each unit [51].

The aim of the present work is to demonstrate the effective detection of different food preservatives, which are compound that are used for the treatment of food to improve the shelf life.

Preprints (www.preprints.org) | NOT PEER-REVIEWED | Posted: 13 May 2019 doi:10.20944/preprints201905.0138.v1

Peer-reviewed version available at Foods 2019, 8, 226; doi:10.3390/foods8060226

For this reason, a novel low-power sensor array was fabricated, which is intended as the heart of a more efficient electronic nose instrument. This portable device could find application as personal safety equipment for food industry workers or for monitoring the quality and the food preservation processes. The proposed array integrates three different types of metal oxide nanowires (SnO_2, CuO and WO_3) on top of commercial μHPs, provided by ams Sensor Solutions Germany GmbH (72770 Reutlingen, Germany). These nanowires were directly synthetized on top of the hotplates using different synthesis techniques, without any transfer of the nanostructures, demonstrating the compatibility of the process with mass production. The morphology and the structure of the sensing materials were investigated briefly, and it was tested the ability of the array to discriminate among different food preservatives: ethanol, acetone, nitrogen dioxide and ozone.

Ethanol is a compound largely found in the food industry, like in food fermentation processes and in alcoholic beverage production [52]. However, is strongly used as preservative to increase shelf life also, as deliberate addition of low concentrations of ethanol inhibits the proliferation of many microorganism, increasing the shelf life of packaged food [53,54]. For example, the addition of ethanol at levels between 0.5% - 3.5% to loaf leads to a substantial extension of the shelf life of bread (more than 1000%) [55].

Acetone, instead, is traditionally used as a solvent in many industrial processes, including Acetone-butanol-ethanol (ABE) fermentation of soluble and hydrolyzed sugars [56], and is one ketones that is present as aroma compound in many foods [57,58]. However, is a well-known interfering compound in the detection of ethanol, as is present in many food processes and is quite different to discriminate from ethanol at low concentrations by artificial olfaction systems.

Nitrogen dioxide is a hazardous compound that has to be monitored in many environmental applications. In the food industry, it is the main source of nitrite, which is a very popular and diffuse compound, for example in aquaculture [59]. In small quantities, it is often added to alcoholic beverages and perishable food like salami, ham and meat [60]. In fact, it is a strong antimicrobial agent, but it can have noxious effects on the human body at concentrations higher than safety standards, binding with haemoglobin and therefore reducing the capability of blood to transport oxygen [61,62]. For drinking water, the US Environmental Protection Agency and the World Health Organization have set a standard of about 3 mg nitrite/L for short-term exposures [61].

Finally, ozone is a compound that attracted a significant interest in the last 30 years due to its role in the atmosphere. However, ozone is used in many industrial fields, including as an alternative to conventional fermentation processes [63] and as a powerful antimicrobial agent [64]. The application of low amounts of ozone (5-10 mg/L) has been tested as an intervention for eliminating pathogens (*Salmonella, E. coli*) from the surface of different seeds and sprouts [65,66], as disinfectant of fruit juices [67] and fresh carrots [68], for example, without leaving residues on food products.

2. Materials and Methods

Commercial state-of-the art μHPs were provided by ams Sensor Solutions Germany GmbH, a leading semiconductor company that recently entered the market of chemical sensors. Micro hotplates are fabricated using planar silicon technology, allowing the preparation of wafers (thickness 450μm) of pre-etched substrates that has to be diced if required (Figure 1, left). Each micro hotplate is 2mm x 2mm size, while the membrane area is 1mm x 1mm with a thickness of only 1μm. Electrodes are deposited on top of the silicon nitride membrane in E120:20 configuration (120μm x 20μm), and the heating element is integrated in the membrane itself. According to the specs, these μHPs can work at up to 450°C for long-term normal operation, and up to 500°C for short bursts if the integrated heating element is used. However, the hotplates were stressed at much higher temperature (up to 870°C) inside the furnace during the synthesis of the nanostructures, and they were able to sustain it without any critical breakdown. This is an excellent result considering the very low thickness and the apparent fragility of the membranes. Figure 1 (right) reports the power versus temperature curve of the integrated heater. For reaching a temperature of 400°C, only 60mW are required. As a comparison, sensors prepared by using 2mm x 2mm alumina substrates, integrated in commercial electronic noses, consume ten times more energy [69].

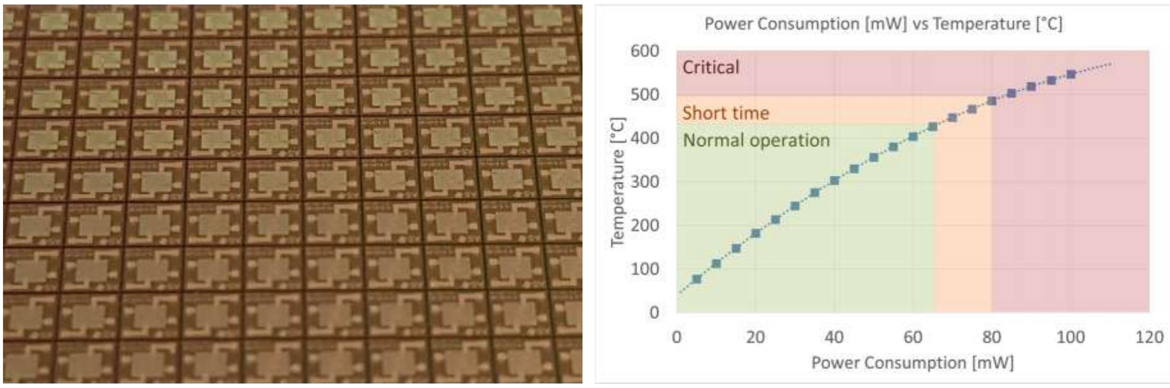

Figure 1: (Left) Optical image of a wafer of ams E120:20 μHPs. (Right) Power consumption versus temperature calibration.

2.1. Synthesis of tungsten trioxide (WO_3) nanowires

Thermal oxidation techniques was used to synthetize tungsten oxide (WO_3) nanowires on ams E120:20 micro hotplates (μHPs). The synthesis process mainly consists in three steps: deposition of metal layer, oxidation and thermal annealing [70].

A thin layer (100nm) of metallic tungsten was deposited on the hotplates by RF magnetron sputtering (100 W argon plasma, 5.5×10^{-3} mbar, room temperature). Afterwards, samples were oxidized in a tubular furnace (custom design based on Lenton furnaces, UK) at 600°C for one hour, in order to grow the nanowires. The pressure inside the alumina tube was set at 0.8 mbar, inletting an argon flow of 10 SCCM by using MKS (Germany) massflow controllers.

After the growing process, samples underwent a thermal annealing to oxidize completely the material [70]. Samples were heated at 400°C for 12 hours in air at atmospheric pressure, in the same tubular furnace.

2.2. Synthesis of copper oxide (CuO) nanowires

The same thermal oxidation technique was used to synthetize copper oxide (CuO) nanowires on μHPs [71], but this time nanowires were synthetized at atmospheric pressure instead of in a vacuum environment.

Firstly, 500nm of metallic copper were deposited on the pre-fabricated electrodes by using RF magnetron sputtering (50 W argon plasma, 5.5×10^{-3} mbar, room temperature). Afterwards, the samples underwent to a forced oxidation in a tubular furnace (Carbolite, UK). Samples were placed in a quartz holder inside the alumina tube at chosen temperature (300°C), gas flow, atmosphere composition and duration. Gas flow was set at 300 SCCM and oxidation time was fixed at 12 hours, in order to obtain a dense mat of nanowires on the surface. The atmosphere inside the furnace consisted in a mixture of argon and oxygen (80% – 20% Ar). The combination of temperature and oxidation time was enough to complete oxidize the material, removing any trace of metallic copper [71].

2.3. Synthesis of tin oxide (SnO_2) nanowires

For the synthesis of tin oxide (SnO_2) nanowires, a custom physical vapor deposition process (PVD) was used. It mainly consists in an evaporation-condensation process based on vapor liquid solid (VLS) mechanism [72–75].

Platinum nanoparticles were deposited on top of the μHPs by DC magnetron sputtering (70 W argon plasma, 5.5x10-3 mbar, room temperature), acting as catalyst seeds for the nucleation of the nanowires. Tin oxide powder (Sigma-Aldrich, 99.9% purity) was dispersed on an alumina holder and put in the middle of the tubular furnace (custom design based on Lenton furnaces, UK), where the

Preprints (www.preprints.org) | NOT PEER-REVIEWED | Posted: 13 May 2019 doi:10.20944/preprints201905.0138.v1

Peer-reviewed version available at Foods 2019, 8, 226; doi:10.3390/foods8060226

temperature is high enough to evaporate the material (1370°C). Substrates were placed in a colder region of the furnace (870°C). At this temperature, the catalytic Pt nanoparticles form droplets that are in liquid form, promoting the condensation of the evaporated material on top of the substrates due to the lower energy required by the process. An argon carrier flow (100sccm, MKS massflow) was used to move the cloud of evaporated material towards the substrates. The pressure inside the furnace was kept at 100mbar and the deposition time was 5 minutes [76].

2.4. Morphological and structural characterization

The morphology of prepared nanowires was investigated by using a field emission scanning electron microscope (FE-SEM model LEO 1525, ZEISS), operated at 3-10 keV energy beam. The microscope was coupled with an Oxford energy dispersive x-ray analysis (EDX), to confirm the elemental composition and the rough stoichiometry of the material. Samples were attached with carbon glue to metallic stubs, to reduce charging effects due to the electron beam.

Raman spectra were measured by using a fiber coupled confocal HORIBA optical microscope at 100x magnification. An iHR320 monochromator was configured with a grating of 1800 g/mm, and was connected to a Peltier-cooled Synapse CCD. A He-Cd blue laser (442 nm) was focused on the samples, to excite the material and promote the Raman scattering. Spectra were recorded in the wavelength range 200-1000 cm^{-1}.

2.5. Device fabrication and functional characterization

The schematic workflow used for the preparation of the sensing devices is reported in Figure 2. In this experimental work, micro-hotplates were diced individually, for greater ease in preparing samples at the prototype level. However, due to the high scalability of the process, all operations could be performed at wafer level, which is a fundamental requirement of a mass-scale production of the devices. After the µHPs dicing, a metal/catalyst layer was deposited by magnetron sputtering, according to the specific metal oxide nanowires, and finally samples were oxidized/underwent VLS process to synthetize the nanowires directly on the hotplates. Functional sensors require a capped hosting case, to interface with the external electronics and to protect the sensing element. Therefore, µHPs were mounted on TO4 package. Pads were connected to TO pins by electro-soldering 50 µm gold wires.

Different devices of the same batches were prepared, and repeated measurements were performed on nominally identical sensors under the same experimental conditions, to evaluate the reproducibility and the yield of the process. The lifetime of the present sensors can be estimated to be > 1 year, over which the samples are still working without any evident deterioration of the surface, exhibiting a small drift (<20%) which is typical of metal oxide materials [77]. It is important to stress that the first cause of device failure is the wrong manipulation: suspended MEMS membrane is very fragile, and could break easily if directly touched. Therefore, samples should be handled with extreme care during wire bonding and during the placing of the protective cap. However, after mounting, sensors are very robust to mechanical stresses, and they are vulnerable mainly only to the thermal shocks if working out of specs, which could results in the breakdown of the membrane or in a permanent damage of the electrodes [47,78,79].

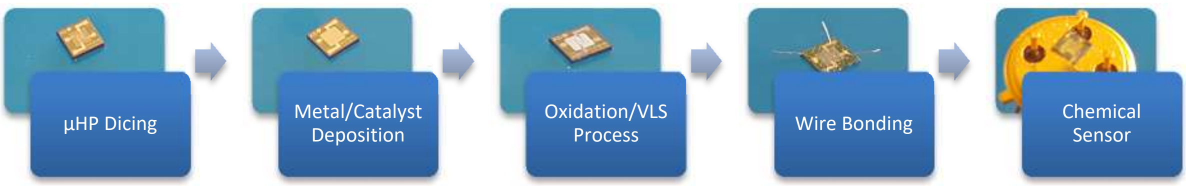

Figure 2: Flow-chart of the integration of MOX nanowires on ams µHPs to fabricate chemical sensors.

To investigate the conductometric response of the sensors, flow-through technique was used. The sensing devices were mounted in a homemade stainless steel test chamber, able to measure up to ten sensors simultaneously [80]. The chamber was set at 20 °C, to avoid the influence of the external

Preprints (www.preprints.org) | NOT PEER-REVIEWED | Posted: 13 May 2019 doi:10.20944/preprints201905.0138.v1

Peer-reviewed version available at Foods 2019, 8, 226; doi:10.3390/foods8060226

temperature. Humidified air was produced by flowing the dry air through a Drechsel bottle, held in a thermostatic bath at 25 °C, and then in a condensation vessel in order to favour the condensation of saturated vapour. The humidified air was mixed with dry air in order to obtain the desired relative humidity (RH) content, in these measurements fixed at 50% @ 20 °C (chamber temperature). Sensor temperatures were controlled by modulating the electric power applied to heaters by Thurlbly-Thandar PL330DP power supplies. A 1 V voltage was applied to the sensors, measuring at the same time the conductance of each sensor using Keithley 6485 picoammetters.

Prior to measurements, samples were thermally stabilized at the optimal working temperature for each chemical compound for 12 hours. Selected gas concentration was let in the chamber for 30 minutes, followed by a restore with synthetic air flow for 90 minutes, to allow the recovery of the baseline. The response of n-type semiconductor sensors is determined by the variation of the conductance, using, for a reducing gas, the following formula:

$$Response = \frac{R_{Gas}-R_{Air}}{R_{Air}} = \frac{G_{Air}-G_{Gas}}{G_{Gas}} \tag{1}$$

and for an oxidizing gas:

$$Response = \frac{G_{Gas}-G_{Air}}{G_{Air}} \tag{2}$$

Where R_{Gas} and G_{Gas} are respectively the resistance and the conductance of the sensor in gas, and R_{Air} and G_{Air} the resistance and the conductance in purified air. For p-type material, the two formulas are swapped.

As specified in the Introduction section, the chemical sensing performance of the fabricated array of sensors were evaluated towards four different chemical compounds which are among the most used food preservers: nitrogen dioxide (NO_2), ethanol (CH_3CH_2OH), acetone ($(CH_3)_2CO$) and ozone (O_3). This allows to highlight the sensing performance and the differences between the materials in the screening of some compounds commonly found in the food industry, demonstrating the capability of the low power array to discriminate among different food preservers. Test gases with a certified composition, supplied by SIAD SpA, (Italy) were mixed in a carrier of dry synthetic air by MKS Instrument mass flow controllers. An UV lamp was used to generate ozone right close to the test chamber, with a maximum concentration of 700ppb. Ozone was then mixed with synthetic air to select the required gas concentration. The total flow inside the chamber was set at 200 SCCM. Short-term reproducibility was taken into account and evaluated for all chemical species and materials. Consecutive measurements were performed at the same concentration and on the same sensor. Results confirm the very good repeatability of the measure, leading to an error less the 10% over four gas injections. All test compound concentrations were selected at much lower values than safety standards, to stress the sensing performances of the portable array.

3. Results and discussion

3.1. Morphological and structural characterization of NWs

Prior to the wire bonding of the micro-hotplates on TO packages, devices were characterized morphologically by optical and FE-SEM microscopy, to confirm the presence of the nanowires, their shape and aspect ratio. In Figure 3 (a) and (b) are reported two optical images of a WO_3 device. Due to the thermal oxidation technique used, nanowires can be patterned easily by simple shadow masking, and they are visible on top of the membrane and on the interdigited electrodes (dark area). Instead, is not possible to control precisely the synthesis of SnO_2 nanowires on the µHPs (Figure 3 (c)), as the VLS mechanism is a random condensation process that cannot be confined properly. The Pt catalyst promotes the growth of the nanowires in some specific regions but, due to the presence of noble metals on the soldering pads, a minor growth happens on pads also. Most of the nanowires are located on the membrane, but this secondary growth on the soldering pads could lead to some issues during the soldering process.

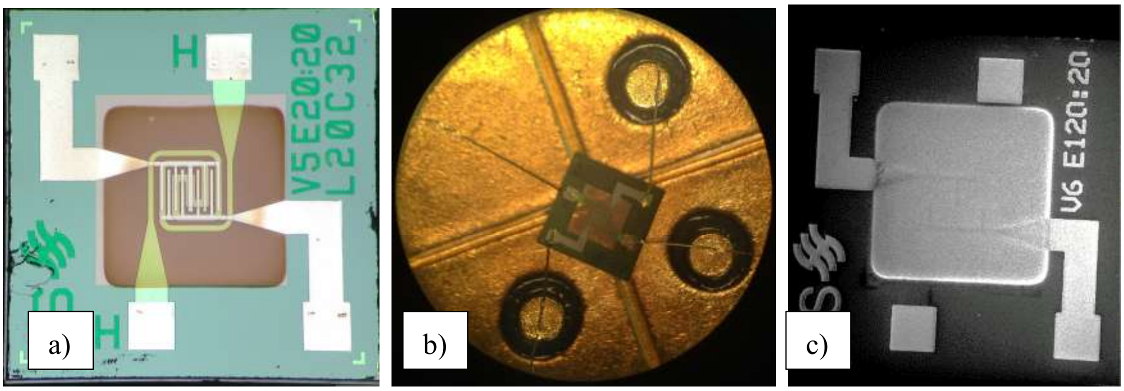

Figure 3: Optical images of WO_3 device as-fabricated **(a)** and mounted with gold wires on TO package **(b)**. Electrodes and heating element are visible through the thin membrane. **(c)** SEM image of SnO_2 device at low magnification (100x).

Figure 4 reports some SEM images of WO_3, CuO and SnO_2 nanowires, at the same magnification level. The density and the dimensions of nanowires are strongly dependant on the material and on the synthesis technique used. Tungsten oxide nanowires are very small and dense, with an average diameter of about 20-30 nm [70]. The mat of copper oxide nanowires is less dense than WO_3, and the average diameter is in the range of 70-100 nm [71]. In case of tin oxide, instead, a dense mat is obtained, but the nanowires are irregular and very long (few μm). It is more difficult to control the geometry of the wires, and thus their diameters are spread over a wide range (100-250nm).

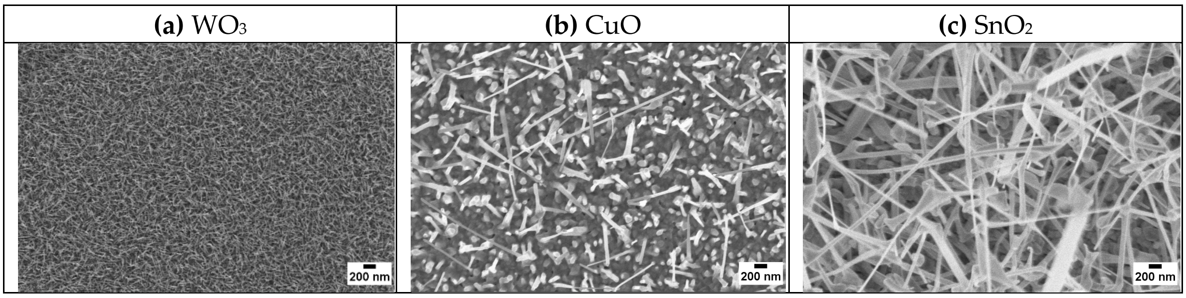

Figure 4: SEM pictures of WO_3 **(a)**, CuO **(b)** and SnO_2 **(c)** nanowires directly synthetized on ams hotplates.

Raman spectroscopy is a not-destructive investigation technique that was used already for the characterization of the thermal properties of μHPs [81]. In this specific case, this powerful technique allows determining the crystalline structure of the sensing material at micrometer size, directly synthetized on top of the hotplate. Indeed, thanks to the focalized laser source is possible to excite only the small area of the metal oxide, confirming that the synthetized nanostructures on the μHPs are crystalline for real. Raman spectra collected from the three different batches of samples are shown in Figure 5.

As reported previously, on tungsten oxide samples the Raman shifts at 260, 322, 703, and 802 cm^{-1} can be attributed mainly to the monoclinic phase of WO_3 (Figure 5, green line) [70,82,83]. The bending vibration of the O-W-O bonds generate the first two shifts. The peaks at 703 and 802 cm^{-1}, instead, correspond to W–O–W stretching vibrations of the bridging oxygen. Raman measurements performed on CuO samples confirm the monoclinic crystalline phase of CuO, commonly found in tenorite rocks (Figure 5, red line). The three predicted Raman active lattice modes are detected at $293 cm^{-1}$ (A_g), $344 cm^{-1}$ (B_g) and $632 cm^{-1}$ (B_g), in line with literature values [84]. Also for the last

Preprints (www.preprints.org) | NOT PEER-REVIEWED | Posted: 13 May 2019 doi:10.20944/preprints201905.0138.v1

Peer-reviewed version available at Foods 2019, 8, 226; doi:10.3390/foods8060226

observed batch of samples, Raman investigations identify shifts that match the one reported in literature for the tetragonal phase of SnO_2 (Cassiterite, Figure 5, blue line) [85]. The three detectable Raman active modes of tin oxide that have been observed are E_g (490 cm^{-1}), A_{1g} (628 cm^{-1}), and B_{2g} (770 cm^{-1}).

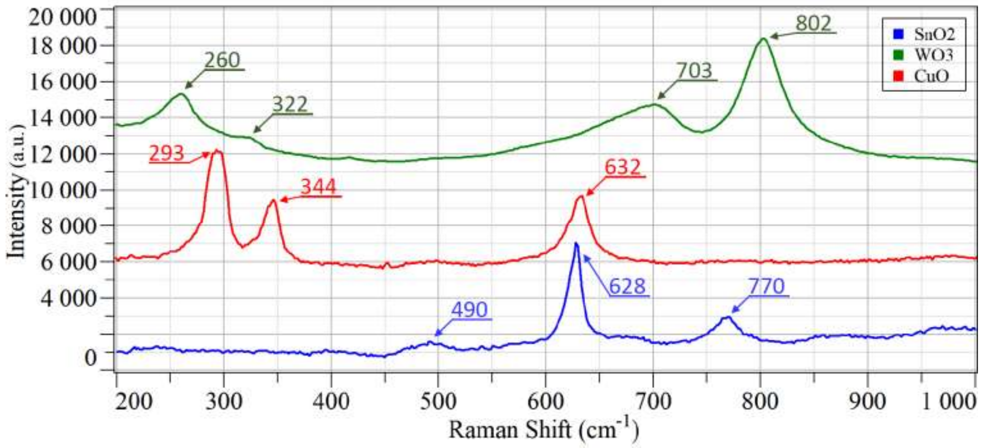

Figure 5: Raman spectra of SnO_2, WO_3 and CuO nanowires deposited on µHPs.

3.1. Chemical sensing performances

As discussed already, the most common working principle of devices integrated in electronic noses is the change of the electrical conductance, due to the interaction of the chemical species in the atmosphere with the surface of the sensing material [86]. Essentially, conductometric chemical sensors works as resistors, in which the electrical resistance of the sensing layer is modulated by the adsorption or interaction of chemical species with the surface. In Figure 6 are shown the electrical conductance of three different devices in presence of ozone, a typical oxidizing gas. The effect of adsorbed species on the surface of the metal oxide depends on the nature of the semiconducting material. In case of n-type materials, such as SnO_2 and WO_3, the presence of a oxidizing gas, like ozone, lead to a reduction of free electrical charge on surface, and thus decreasing the overall electrical conductance. In p-type material like CuO, instead, the presence of oxidizing gas lead to an increase of the conductance [87].

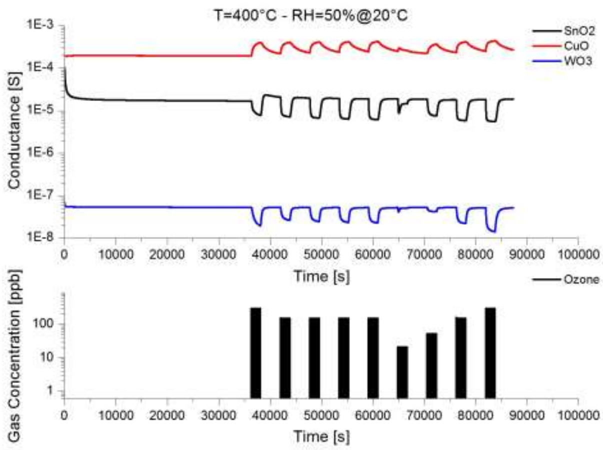

Figure 6: Dynamic response of SnO_2, CuO and WO_3 nanowires in presence of different concentration of Ozone (300-150-150-150-150-20-50-150-300 ppb, respectively). Operating temperature for all sensing devices was 400°C. Relative humidity was 50%@20°C.

From the dynamic measure is possible to observe the excellent stability of the baseline of all three different devices at constant power mode, even during long-time operation. This is a fundamental requirement for the integration of reliable sensors into electronic noses: a frequent sensors calibration is undesired because it requires personnel attendance, cannot be automated and force the instrument to stop [46]. Figure 6 shows also an example of the very good reproducibility of the measure. The response profile of four consecutive ozone injections is almost identical in all samples, exhibiting an error less than 10% in short term investigations. Moreover, all devices completely recover the baseline, with no sign of surface contaminations or damaging even in presence of a reactive gas like ozone, which is known to be a very strong oxidizer.

In electronic noses, each sensor of the array can be powered at the desired temperature, according to the specific compounds fingerprints to detect. According to micro hotplate specifications, investigations were limited to 400°C to avoid any damage during long-time operation, like for example membrane breakdown caused by thermal stress. In this specific case, a temperature of 400°C was selected as the optimal one for the detection of ethanol, acetone and ozone, while for nitrogen dioxide 200°C is chosen. These values are in line with previous investigations [70,71,76].

Each metal oxides deposited on the μHPs have different physical and electrical properties, related to the surface chemistry and the defects in the crystalline structure [88]. Therefore, different sensor responses in presence of a specific concentration of the target compounds are expected. To understand which is the most sensitive material towards each compound, the performances of the devices were compared directly at the same concentrations, as reported in Figure 7. The interest is to measure very low NO_2 concentrations, which are quite difficult to detect with these kind of devices [89]. Among the three metal oxide devices investigated, only WO_3 was able to produce an appreciable response towards 100ppb of NO_2, a concentration much lower than the safety standard requirements. This result is not unexpected, tungsten trioxide is well known in literature to have good sensing performance in detecting nitrogen dioxide [90]. Tin and copper oxide responses, instead, were negligible. The asymmetry of the response between different materials is the key feature of electronic noses, because helps patter recognition methods in the discrimination between different compounds.

Tin oxide is mostly suited, in these tests, to detect VOCs such as ethanol and acetone. Interestingly, SnO_2 is more sensitive to ethanol than acetone at the same concentration of 30ppm. On the contrary, WO_3 is more sensitive to acetone, even if its overall response is lower than SnO_2. CuO was not able to compete with the other two materials in term of response, but does not seem to prefer neither ethanol nor acetone. Again, the different behaviour of the metal oxides in VOCs sensing allow a more efficient discrimination. About ozone, tungsten trioxide is the most sensitive material toward a concentration of 300ppb, followed by tin oxide. On the other hand, copper oxide response is significantly lower.

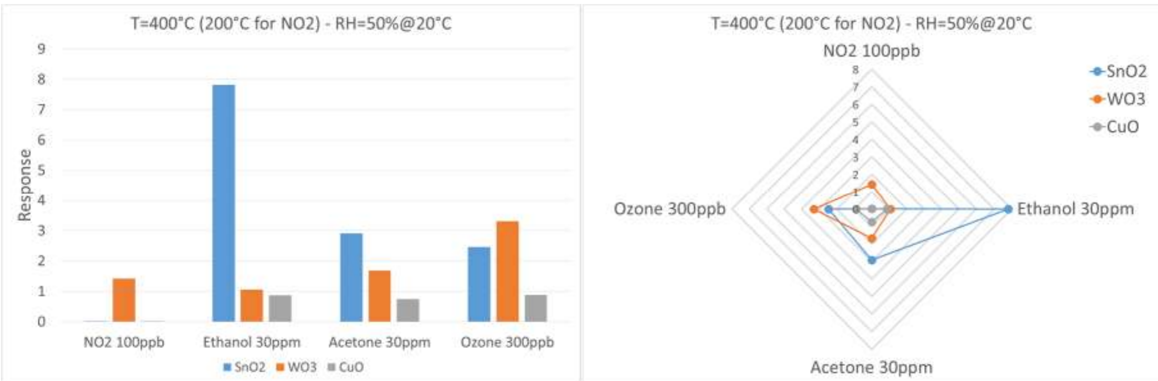

Figure 7: Comparison of different sensing materials towards specific concentrations of target chemical compounds. Operating temperature for all sensing devices was 400°C towards ethanol, acetone and ozone, while it was 200°C for nitrogen dioxide. Relative humidity was 50%@20°C.

In Figure 8, the responses of each different sensing materials in presence of various concentrations of target compounds is reported. Dashed lines in Figure 8 refer to a power-law fitting of data points, according to the typical formula:

$$\text{Response}=A[\text{gas concentration}]^{B} \quad (3)$$

Where A and B are constants depending on the material and the target chemical species. Each data point is the average response of at least three different sensors from the same batch, nominally identical. Error bars refer to intrinsic measured variability between devices.

Calibration curves confirm the better performances of WO_3 in detecting NO_2, outperforming both tin oxide and copper oxide, which was not even reported due to very low response. Defining the detection limit of the devices as the gas concentration producing a unitary response (Response=1), ≈100ppb is identified as the limit for nitrogen dioxide.

Moving to VOCs, calibration curves confirm the higher responses of SnO_2 devices, especially towards ethanol. Detection limits, previously defined, are estimated as ≈5ppm for ethanol and ≈15ppm for acetone. However, an increased variability in the response of different tin oxide device is reported. This could be related to the synthesis process: it is more difficult to control the morphology and dimensions of the nanowires, and this is reflected in sensor response. Tungsten and copper oxide devices perform worse, but responses from different devices of the same batch are more consistent.

Ozone sensing shows mixed results. For high ozone concentration (>200ppb) tungsten oxide devices exhibit better performance compared to tin and copper oxides. At moderate and low ozone concentrations (<200ppb) instead, tin oxide outperform tungsten oxide devices. Copper oxide response is always less than other two type of sensing devices. Detection limit for tin oxide devices is estimated at ≈40ppb. Detection limits of the three different materials toward specific target compounds are reported in Figure 9.

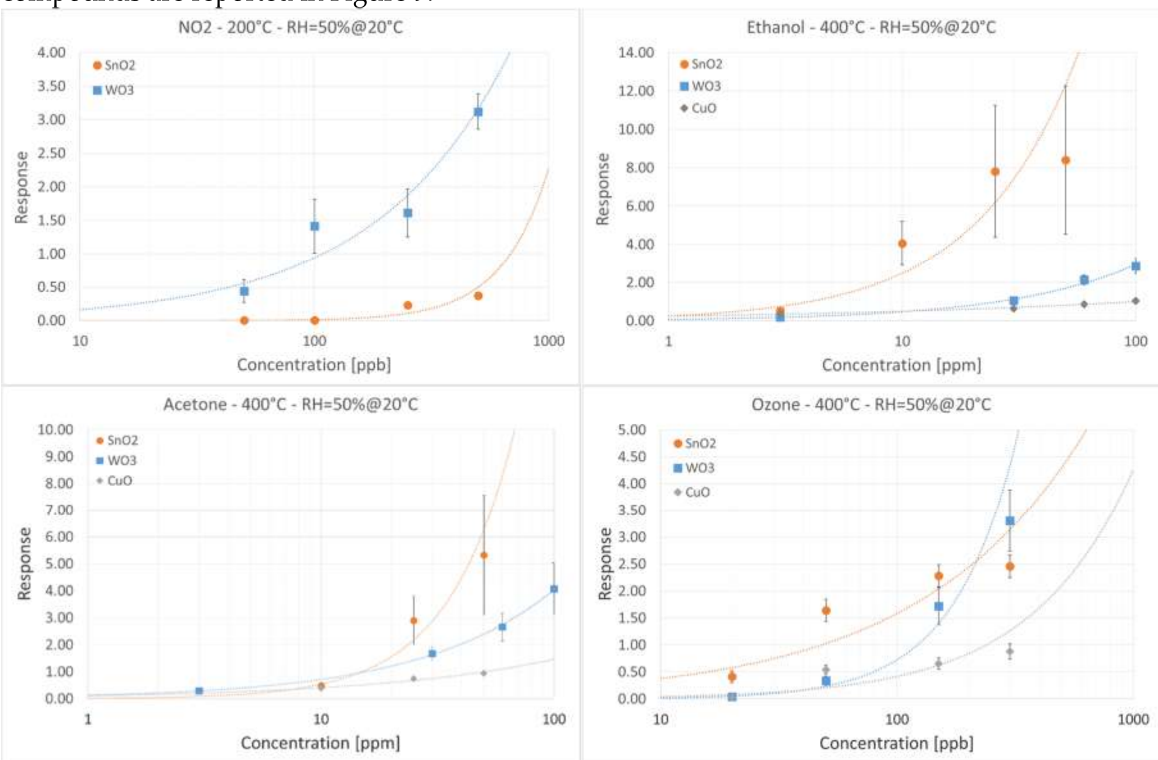

Figure 8: Calibration curves in presence of different chemical species: NO2, Ethanol, Acetone and Ozone. Relative humidity was 50%@20°C.

	NO2	Ethanol	Acetone	Ozone
SnO2	>1ppm	5ppm	15ppm	40ppb
WO3	100ppb	25ppm	15ppm	150ppb
CuO	>1ppm	40ppm	50ppm	300ppb

Figure 9: Detection limits of the three different materials toward target chemical compounds

Principal Component Analysis (PCA) is by far the most used unsupervised data algorithm to manage the information coming from an electronic nose. It mainly consists in a linear extraction technique that reduces data dimensionality with a minimum loss of information, projecting them into lower dimensions (usually 2 or 3) [24]. Figure 10 reports a PCA analysis performed using the data previously presented. As expected, efficient discrimination between ethanol and acetone is very difficult using only the three sensors integrated in the array. Therefore, acetone has not been included in this representation. However, is it possible to add new sensors to the array when integrated in the electronic noses, increasing the number of different sensors even up to thousands, which allows more likely the discrimination of specific fingerprints [86]. Nevertheless, WO_3, SnO_2 and CuO devices were able to discriminate between ethanol, ozone and nitrogen dioxide at low concentrations, demonstrating the capability of the fabricated sensor array to distinguish the correct food preserver.

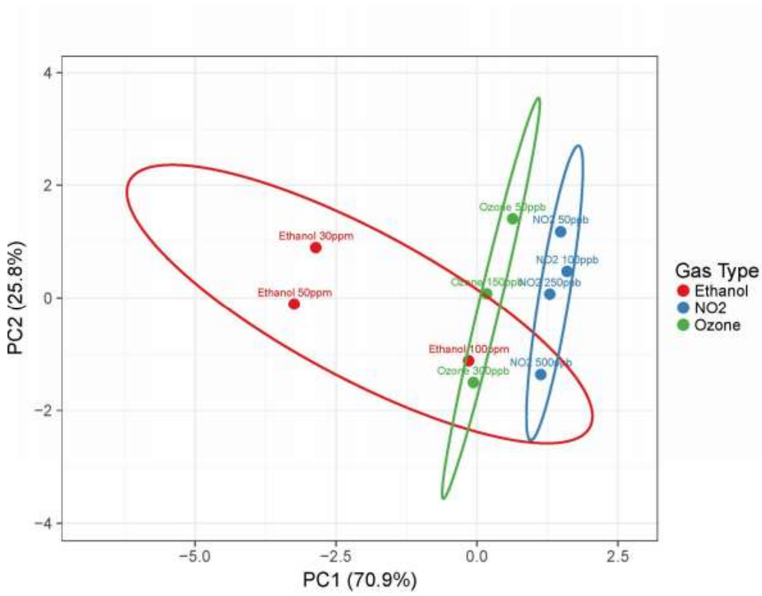

Figure 10: Pareto scaling is applied to rows; SVD with imputation is used to calculate principal components. X and Y axis show principal component 1 and principal component 2 that explain 70.9% and 25.8% of the total variance, respectively. Prediction ellipses are such that with probability 0.95, a new observation from the same group will fall inside the ellipse. N = 10 data points.

4. Conclusions

Electronic olfaction systems are becoming used largely in the food safety and security fields, due to high reliability, low cost, easy use and the possibility of on-line monitoring. While research is focusing on the enhancements of their performances to promote further the use of such systems in the food industry, a special attention is devoted to reduce the power consumption of each single sensor, to allow the fabrication of portable or battery operated equipment.

In this work, a simple sensor array based on copper, tin and tungsten oxide nanowires was prepared, and its performances in the detection of common food preservatives were evaluated. The nanowires in the sensing array were synthetized on commercial low power micro-hotplates from ams Sensor Solutions Germany GmbH (Germany). This novel sensor array combines the advantages of

Preprints (www.preprints.org) | NOT PEER-REVIEWED | Posted: 13 May 2019 doi:10.20944/preprints201905.0138.v1

Peer-reviewed version available at *Foods* **2019**, *8*, 226; doi:10.3390/foods8060226

conductometric metal oxides together with the increased sensing performances of nanowire technology and the reduced power consumption from silicon MEMS technology. The three sensing materials were characterized, to investigate the morphology and the structure of synthetized nanowires, by using FE-SEM, XRD and Raman spectroscopy.

The fabricated array was testes towards four different food preservatives commonly used in the food industry, specifically nitrogen dioxide, ethanol, acetone and ozone. Tungsten oxide resulted as the most sensing material to detect nitrogen dioxide, even in low concentration (100ppb). Tin oxide, instead, showed higher performance in detecting VOCs such as ethanol and acetone. The response of copper oxide devices was always less than other two material, but still measurable.

Results confirm the ability of the sensing array to detect concentrations of food preservers that are much smaller than safety standard requirements. The sensing performance of these different materials resulted complementary: the combination of all sensor readouts may provide significant information when integrated as in arrays or e-noses. Moreover, the use of a common technological platform allows the mass production of these sensors, helping to reduce the fabrication costs. Finally, the very small thermal inertia of the micro hotplates allows fancy operating modes, such as discontinuous operation or pulsed temperature [48]. This is considered the frontier of sampling, because not only reduces further the power consumption of the system, but enables also the use of more advanced data algorithms such as advanced fuzzy and pattern recognition, which can give a boost in the accuracy of the fingerprint and aroma recognition [91].

Supplementary Materials: No supplementary materials.

Funding: This work was supported by the European Community's 7th Framework Programme, under the grant agreement n° 611887 "MSP: Multi Sensor Platform for Smart Building Management".

Acknowledgments: The author would like to thank Martin Herold (ams Sensor Solutions Germany GmbH, 72770 Reutlingen, Germany) for providing the micro hotplates. Moreover, the author thanks all SENSOR Laboratory staff and personnel.

Author Contributions: D.Z. conceived the work, designed & performed the experiments and wrote the manuscript.

Conflicts of Interest: The authors declare no conflict of interest.

References

1. Low, K.E.Y. Ruminations on Smell as a Sociocultural Phenomenon. *Curr. Sociol.* **2005**, *53*, 397–417.
2. Kelley, J.L.; Magurran, A.E. Learned predator recognition and antipredator responses in fishes. *Fish Fish.* **2003**, *4*, 216–226.
3. Firestein, S. How the olfactory system makes sense of scents. *Nature* **2001**, *413*, 211–218.
4. Richardson, J.T.E.; Zucco, G.M. Cognition and Olfaction: A Review. *Psychol. Bull.* **1989**, *105*, 352–360.
5. Röck, F.; Barsan, N.; Weimar, U. Electronic nose: Current status and future trends. *Chem. Rev.* **2008**, *108*, 705–725.
6. Sankaran, S.; Khot, L.R.; Panigrahi, S. Biology and applications of olfactory sensing system: A review. *Sensors Actuators B Chem.* **2012**, *171–172*, 1–17.
7. Brattoli, M.; De Gennaro, G.; De Pinto, V.; Demarinis Loiotile, A.; Lovascio, S.; Penza, M. Odour Detection Methods: Olfactometry and Chemical Sensors. *Sensors* **2011**, *11*, 5290–5322.
8. Zampolli, S.; Elmi, I.; Ahmed, F.; Passini, M.; Cardinali, G.C.; Nicoletti, S.; Dori, L. An electronic nose based on solid state sensor arrays for low-cost indoor air quality monitoring applications. *Sensors Actuators B Chem.* **2004**, *101*, 39–46.
9. Wolfrum, E.J.; Meglen, R.M.; Peterson, D.; Sluiter, J. Metal oxide sensor arrays for the detection, differentiation, and quantification of volatile organic compounds at sub-parts-per-million concentration

levels. *Sensors Actuators B Chem.* **2006**, *115*, 322–329.

10. Szulczyński, B.; Wasilewski, T.; Wojnowski, W.; Majchrzak, T.; Dymerski, T.; Namieśnik, J.; Gębicki, J. Different Ways to Apply a Measurement Instrument of E-Nose Type to Evaluate Ambient Air Quality with Respect to Odour Nuisance in a Vicinity of Municipal Processing Plants. *Sensors* **2017**, *17*.
11. Wu, Y.; Liu, T.; Ling, S.H.; Szymanski, J.; Zhang, W.; Su, S.W. Air Quality Monitoring for Vulnerable Groups in Residential Environments Using a Multiple Hazard Gas Detector. *Sensors* **2019**, *19*.
12. Haddi, Z.; Amari, A.; Alami, H.; Bari, N. El; Llobet, E.; Bouchikhi, B. A portable electronic nose system for the identification of cannabis-based drugs. *Sensors Actuators B Chem.* **2011**, *155*, 456–463.
13. Huang, C.-H.; Zeng, C.; Wang, Y.-C.; Peng, H.-Y.; Lin, C.-S.; Chang, C.-J.; Yang, H.-Y. A Study of Diagnostic Accuracy Using a Chemical Sensor Array and a Machine Learning Technique to Detect Lung Cancer. *Sensors* **2018**, *18*.
14. Scarlata, S.; Finamore, P.; Santangelo, S.; Giannunzio, G.; Pennazza, G.; Grasso, S.; Santonico, M.; Incalzi, R.A. Cluster analysis on breath print of newly diagnosed {COPD} patients: effects of therapy. *J. Breath Res.* **2018**, *12*, 36022.
15. Wilson, A.D.; Baietto, M. Advances in Electronic-Nose Technologies Developed for Biomedical Applications. *Sensors* **2011**, *11*, 1105–1176.
16. Wijaya, D.R.; Sarno, R.; Zulaika, E. Electronic nose dataset for beef quality monitoring in uncontrolled ambient conditions. *Data Br.* **2018**, *21*, 2414–2420.
17. Macías, M.M.; Manso, A.G.; Orellana, C.J.G.; Velasco, H.M.G.; Caballero, R.G.; Chamizo, J.C.P. Acetic Acid Detection Threshold in Synthetic Wine Samples of a Portable Electronic Nose. *Sensors* **2013**, *13*, 208–220.
18. Hasan, N.U.; Ejaz, N.; Ejaz, W.; Kim, H.S. Meat and Fish Freshness Inspection System Based on Odor Sensing. *Sensors* **2012**, *12*, 15542–15557.
19. Moncrieff, R.W. An instrument for measuring and classifying odors. *J. Appl. Physiol.* **1961**, *16*, 742–749.
20. WILKENS, W.F.; HARTMAN, J.D. An Electronic Analog for the Olfactory Processesa. *J. Food Sci.* **1964**, *29*, 372–378.
21. Persaud, K.; Dodd, G. Analysis of discrimination mechanisms in the mammalian olfactory system using a model nose. *Nature* **1982**, *299*, 352–355.
22. Núñez Carmona, E.; Sberveglieri, V.; Ponzoni, A.; Galstyan, V.; Zappa, D.; Pulvirenti, A.; Comini, E. Detection of food and skin pathogen microbiota by means of an electronic nose based on metal oxide chemiresistors. *Sensors Actuators, B Chem.* **2017**, *238*.
23. Núñez-Carmona, E.; Abbatangelo, M.; Sberveglieri, V. Innovative Sensor Approach to Follow Campylobacter jejuni Development. *Biosensors* **2019**, *9*.
24. Peris, M.; Escuder-Gilabert, L. A 21st century technique for food control: Electronic noses. *Anal. Chim. Acta* **2009**, *638*, 1–15.
25. LaBorde, L.F. HACCP and HACCP-Based Programs for Controlling Food Safety Hazards in the Vegetable Industry. In *Handbook of Vegetables and Vegetable Processing*; John Wiley & Sons, Ltd, 2018; pp. 969–987 ISBN 9781119098935.
26. Mariana, R.R.; Hidayati, L.; Soekopitojo, S. Implementing the HACCP system to the production of Bakso Malang-Indonesia. *J. Culin. Sci. Technol.* **2018**, *0*, 1–22.
27. Feng, H.; Chen, J.; Zhou, W.; Rungsardthong, V.; Zhang, X. Modeling and evaluation on WSN-enabled and knowledge-based HACCP quality control for frozen shellfish cold chain. *Food Control* **2019**, *98*, 348–358.

Peer-reviewed version available at *Foods* **2019**, *8*, 226; doi:10.3390/foods8060226

28. Gliszczyńska-Świgło, A.; Chmielewski, J. Electronic Nose as a Tool for Monitoring the Authenticity of Food. A Review. *Food Anal. Methods* **2017**, *10*, 1800–1816.
29. Abbatangelo, M.; Núñez-Carmona, E.; Duina, G.; Sberveglieri, V. Multidisciplinary Approach to Characterizing the Fingerprint of Italian EVOO. *Molecules* **2019**, *24*.
30. Abbatangelo, M.; Núñez-Carmona, E.; Sberveglieri, V.; Zappa, D.; Comini, E.; Sberveglieri, G. Application of a novel S3 nanowire gas sensor device in parallel with GC-MS for the identification of rind percentage of grated Parmigiano Reggiano. *Sensors (Switzerland)* **2018**, *18*.
31. Wang, M.; Gao, F.; Wu, Q.; Zhang, J.; Xue, Y.; Wan, H.; Wang, P. Real-time assessment of food freshness in refrigerators based on a miniaturized electronic nose. *Anal. Methods* **2018**, *10*, 4741–4749.
32. Ramírez, H.L.; Soriano, A.; Gómez, S.; Iranzo, J.U.; Briones, A.I. Evaluation of the Food Sniffer electronic nose for assessing the shelf life of fresh pork meat compared to physicochemical measurements of meat quality. *Eur. Food Res. Technol.* **2018**, *244*, 1047–1055.
33. Popping, B.; De Dominicis, E.; Dante, M.; Nocetti, M. Identification of the Geographic Origin of Parmigiano Reggiano (P.D.O.) Cheeses Deploying Non-Targeted Mass Spectrometry and Chemometrics. *Foods* **2017**, *6*.
34. Maout, P. Le; Wojkiewicz, J.-L.; Redon, N.; Lahuec, C.; Seguin, F.; Dupont, L.; Mikhaylov, S.; Noskov, Y.; Ogurtsov, N.; Pud, A. Polyaniline nanocomposites based sensor array for breath ammonia analysis. Portable e-nose approach to non-invasive diagnosis of chronic kidney disease. *Sensors Actuators B Chem.* **2018**, *274*, 616–626.
35. Vergara, A.; Fonollosa, J.; Mahiques, J.; Trincavelli, M.; Rulkov, N.; Huerta, R. On the performance of gas sensor arrays in open sampling systems using Inhibitory Support Vector Machines. *Sensors Actuators B Chem.* **2013**, *185*, 462–477.
36. Magna, G.; Zor, S.D.; Catini, A.; Capuano, R.; Basoli, F.; Martinelli, E.; Paolesse, R.; Natale, C. Di Surface arrangement dependent selectivity of porphyrins gas sensors. *Sensors Actuators B Chem.* **2017**, *251*, 524–532.
37. Catini, A.; Kumar, R.; Capuano, R.; Martinelli, E.; Paolesse, R.; Di Natale, C. An Exploration of the Metal Dependent Selectivity of a Metalloporphyrins Coated Quartz Microbalances Array. *Sensors* **2016**, *16*.
38. Jeong, Y.; Shin, J.; Hong, Y.; Wu, M.; Hong, S.; Kwon, K.C.; Choi, S.; Lee, T.; Jang, H.W.; Lee, J.-H. Gas sensing characteristics of the FET-type gas sensor having inkjet-printed WS2 sensing layer. *Solid. State. Electron.* **2019**, *153*, 27–32.
39. Natale, C. Di; Martinelli, E.; Paolesse, R.; D'Amico, A.; Filippini, D.; Lundström, I. An artificial olfaction system based on the optical imaging of a large array of chemical reporters. *Sensors Actuators B Chem.* **2009**, *142*, 412–417.
40. Tonezzer, M.; Dang, L.T.T.; Tran, H.Q.; Iannotta, S. Multiselective visual gas sensor using nickel oxide nanowires as chemiresistor. *Sensors Actuators B Chem.* **2018**, *255*, 2785–2793.
41. Yamazoe, N. New approaches for improving semiconductor gas sensors. *Sensors Actuators B Chem.* **1991**, *5*, 7–19.
42. BARSAN, N.; KOZIEJ, D.; WEIMAR, U. Metal oxide-based gas sensor research: How to? *Sensors Actuators B Chem.* **2007**, *121*, 18–35.
43. Comini, E.; Sberveglieri, G. Metal oxide nanowires as chemical sensors. *Mater. Today* **2010**, *13*, 36–44.
44. Rakshit, T.; Santra, S.; Manna, I.; Ray, S.K. Enhanced sensitivity and selectivity of brush-like SnO_2 nanowire/ZnO nanorod heterostructure based sensors for volatile organic compounds. *RSC Adv.* **2014**, *4*, 36749.

45. Comini, E. Metal oxide nanowire chemical sensors: innovation and quality of life. *Mater. Today* **2016**, *19*, 559–567.
46. Romain, A.C.; Nicolas, J. Long term stability of metal oxide-based gas sensors for e-nose environmental applications: An overview. *Sensors Actuators B Chem.* **2010**, *146*, 502–506.
47. Udrea, F.; Gardner, J.W.; Setiadi, D.; Covington, J.A.; Dogaru, T.; Lu, C.C.; Milne, W.I. Design and simulations of SOI CMOS micro-hotplate gas sensors. *Sensors Actuators B Chem.* **2001**, *78*, 180–190.
48. Vergara, A.; Ramírez, J.L.; Llobet, E. Reducing power consumption via a discontinuous operation of temperature-modulated micro-hotplate gas sensors: Application to the logistics chain of fruit. *Sensors Actuators B Chem.* **2008**, *129*, 311–318.
49. Vergara, A.; Llobet, E.; Brezmes, J.; Ivanov, P.; Vilanova, X.; Gracia, I.; Cané, C.; Correig, X. Optimised temperature modulation of metal oxide micro-hotplate gas sensors through multilevel pseudo random sequences. *Sensors Actuators B Chem.* **2005**, *111–112*, 271–280.
50. Kunt, T.A.; McAvoy, T.J.; Cavicchi, R.E.; Semancik, S. Optimization of temperature programmed sensing for gas identification using micro-hotplate sensors. *Sensors Actuators B Chem.* **1998**, *53*, 24–43.
51. Viricelle, J.-P.; Pijolat, C.; Riviere, B.; Rotureau, D.; Briand, D.; de Rooij, N.F. Compatibility of screen-printing technology with micro-hotplate for gas sensor and solid oxide micro fuel cell development. *Sensors Actuators B Chem.* **2006**, *118*, 263–268.
52. Adley, C.C. Past, Present and Future of Sensors in Food Production. *Foods* **2014**, *3*, 491–510.
53. Katsinis, G.; Rigas, F.; Doulia, D. Synergistic effect of chemical preservatives with ethanol on the microbial shelf life of bread by factorial design. *Int. J. Food Sci. Technol.* **2008**, *43*, 208–215.
54. Kalathenos, P.; Russell, N.J. Ethanol as a food preservative. In *Food Preservatives*; Russell, N.J., Gould, G.W., Eds.; Springer US: Boston, MA, 2003; pp. 196–217 ISBN 978-0-387-30042-9.
55. Doulia, D.; Katsinis, G.; Mougin, B. Prolongation of the microbial shelf life of wrapped part baked baguettes. *Int. J. Food Prop.* **2000**, *3*, 447–457.
56. Jin, Q.; Qureshi, N.; Wang, H.; Huang, H. Acetone-butanol-ethanol (ABE) fermentation of soluble and hydrolyzed sugars in apple pomace by Clostridium beijerinckii P260. *Fuel* **2019**, *244*, 536–544.
57. Bai, J.; Baker, S.M.; Goodrich-Schneider, R.M.; Montazeri, N.; Sarnoski, P.J. Aroma Profile Characterization of Mahi-Mahi and Tuna for Determining Spoilage Using Purge and Trap Gas Chromatography-Mass Spectrometry. *J. Food Sci.* **2019**, *84*, 481–489.
58. Rashid, A.; Javed, I.; Rasco, B.; Sablani, S.; Ayaz, M.; Ali, M.A.; Abdullah, M.; Imran, M.; Gondal, T.A.; Afzal, M.I.; et al. Measurement of Off-Flavoring Volatile Compounds and Microbial Load as a Probable Marker for Keeping Quality of Pasteurized Milk. *Appl. Sci.* **2019**, *9*.
59. Silfiana; Widowati; Putro, S.P.; Udjiani, T. Modeling of nitrogen transformation in an integrated multi-trophic aquaculture ({IMTA}). *J. Phys. Conf. Ser.* **2018**, *983*, 12122.
60. Manikandan, V.S.; Liu, Z.; Chen, A. Simultaneous detection of hydrazine, sulfite, and nitrite based on a nanoporous gold microelectrode. *J. Electroanal. Chem.* **2018**, *819*, 524–532.
61. Eytcheson, S.A.; LeBlanc, G.A. Hemoglobin Levels Modulate Nitrite Toxicity to Daphnia magna. *Sci. Rep.* **2018**, *8*, 7172.
62. Hathazi, D.; Scurtu, F.; Bischin, C.; Mot, A.; Attia, A.A.A.; Kongsted, J.; Silaghi-Dumitrescu, R. The Reaction of Oxy Hemoglobin with Nitrite: Mechanism, Antioxidant-Modulated Effect, and Implications for Blood Substitute Evaluation. *Molecules* **2018**, *23*.
63. Junior, M.D.M.; Castanha, N.; dos Anjos, C.B.P.; Augusto, P.E.D.; Sarmento, S.B.S. Ozone technology as an alternative to fermentative processes to improve the oven-expansion properties of cassava starch.

Food Res. Int. **2019**, *123*, 56–63.

64. Khadre, M.A.; Yousef, A.E.; Kim, J.-G. Microbiological Aspects of Ozone Applications in Food: A Review. *J. Food Sci.* **2001**, *66*, 1242–1252.
65. Sharma, R.R.; Demirci, A.; Puri, V.M.; Beuchat, L.R.; Fett, W.F. Modeling the inactivation of Escherichia coli O157:H7 on inoculated alfalfa seeds during exposure to ozonated or electrolyzed oxidizing water. *Trans. Am. Soc. Agric. Eng.* **2004**, *47*, 173–181.
66. Mohammad, Z.; Kalbasi-Ashtari, A.; Riskowski, G.; Castillo, A. Reduction of Salmonella and Shiga toxin-producing Escherichia coli on alfalfa seeds and sprouts using an ozone generating system. *Int. J. Food Microbiol.* **2019**, *289*, 57–63.
67. Shah, N.N.A.K.; Supian, N.A.M.; Hussein, N.A. Disinfectant of pummelo (Citrus Grandis L. Osbeck) fruit juice using gaseous ozone. *J. Food Sci. Technol.* **2019**, *56*, 262–272.
68. Evrendilek, G.A.; Ozdemir, P. Effect of various forms of non-thermal treatment of the quality and safety in carrots. *LWT* **2019**, *105*, 344–354.
69. Abbatangelo, M.; Núñez-Carmona, E.; Sberveglieri, V. Application of a novel S3 nanowire gas sensor device in parallel with GC-MS for the identification of Parmigiano Reggiano from US and European competitors. *J. Food Eng.* **2018**, *236*, 36–43.
70. Zappa, D.; Bertuna, A.; Comini, E.; Molinari, M.; Poli, N.; Sberveglieri, G. Tungsten oxide nanowires for chemical detection. *Anal. Methods* **2015**, *7*, 2203–2209.
71. Zappa, D.; Comini, E.; Zamani, R.; Arbiol, J.; Morante, J.R.; Sberveglieri, G. Preparation of copper oxide nanowire-based conductometric chemical sensors. *Sensors Actuators B Chem.* **2013**, *182*, 7–15.
72. Roper, S.M.; Davis, S.H.; Norris, S.A.; Golovin, A.A.; Voorhees, P.W.; Weiss, M. Steady growth of nanowires via the vapor-liquid-solid method. *J. Appl. Phys.* **2007**, *102*, 034304.
73. Her, Y.-C.; Chiang, C.-K.; Jean, S.-T.; Huang, S.-L. Self-catalytic growth of hierarchical In_2O_3 nanostructures on SnO_2 nanowires and their CO sensing properties. *CrystEngComm* **2012**, *14*, 1296–1300.
74. Kaur, N.; Zappa, D.; Ferroni, M.; Poli, N.; Campanini, M.; Negrea, R.; Comini, E. Branch-like NiO/ZnO heterostructures for VOC sensing. *Sensors Actuators, B Chem.* **2018**, *262*.
75. Kolasinski, K.W. Catalytic growth of nanowires: Vapor–liquid–solid, vapor–solid–solid, solution–liquid–solid and solid–liquid–solid growth. *Curr. Opin. Solid State Mater. Sci.* **2006**, *10*, 182–191.
76. Comini, E.; Faglia, G.; Sberveglieri, G.; Pan, Z.; Wang, Z.L. Stable and highly sensitive gas sensors based on semiconducting oxide nanobelts. *Appl. Phys. Lett.* **2002**, *81*, 1869–1871.
77. Korotcenkov, G.; Cho, B.K. Instability of metal oxide-based conductometric gas sensors and approaches to stability improvement (short survey). *Sensors Actuators B Chem.* **2011**, *156*, 527–538.
78. Puigcorb, J.; Vogel, D.; Michel, B.; Vil, A.; Gr cia, I.; Can, C.; Morante, J.R. High temperature degradation of Pt/Ti electrodes in micro-hotplate gas sensors. *J. Micromechanics Microengineering* **2003**, *13*, S119–S124.
79. Gardner, J.W.; Pike, A.; de Rooij, N.F.; Koudelka-Hep, M.; Clerc, P.A.; Hierlemann, A.; Göpel, W. Integrated array sensor for detecting organic solvents. *Sensors Actuators B Chem.* **1995**, *26*, 135–139.
80. Sberveglieri, G.; Faglia, G.; Perego, C.; Nelli, P.; Marks, R.N.; Virgili, T.; Taliani, C.; Zamboni, R. Hydrogen and humidity sensing properties of C60 thin films. *Synth. Met.* **1996**, *77*, 273–275.
81. Deluca, M.; Wimmer-Teubenbacher, R.; Mitterhuber, L.; Mader, J.; Rohracher, K.; Holzer, M.; Köck, A. In-Situ Temperature Measurement on CMOS Integrated Micro-Hotplates for Gas Sensing Devices. *Sensors* **2019**, *19*.
82. Sadek, A.Z.; Zheng, H.; Breedon, M.; Bansal, V.; Bhargava, S.K.; Latham, K.; Zhu, J.; Yu, L.; Hu, Z.; Spizzirri, P.G.; et al. High-Temperature Anodized WO_3 Nanoplatelet Films for Photosensitive Devices.

Peer-reviewed version available at *Foods* **2019**, *8*, 226; doi:10.3390/foods8060226

Langmuir **2009**, *25*, 9545–9551.

83. Zheng, H.; Tachibana, Y.; Kalantar-zadeh, K. Dye-Sensitized Solar Cells Based on WO_3. *Langmuir* **2010**, *26*, 19148–19152.
84. Hagemann, H.; Bill, H.; sadowski, W.; Walker, E.; François, M. Raman spectra of single crystal CuO. *Solid State Commun.* **1990**, *73*, 447–451.
85. Marina N. Rumyantseva, †; Alexander M. Gaskov, †; N. Rosman, ‡; T. Pagnier, ‡ and; Juan R. Morante*, § Raman Surface Vibration Modes in Nanocrystalline SnO2: Correlation with Gas Sensor Performances. **2005**.
86. Chiu, S.-W.; Tang, K.-T. Towards a Chemiresistive Sensor-Integrated Electronic Nose: A Review. *Sensors* **2013**, *13*, 14214–14247.
87. Barsan, N.; Simion, C.; Heine, T.; Pokhrel, S.; Weimar, U. Modeling of sensing and transduction for p-type semiconducting metal oxide based gas sensors. *J. Electroceramics* **2010**, *25*, 11–19.
88. Arafat, M.M.; Dinan, B.; Akbar, S.A.; Haseeb, A.S.M.A. Gas Sensors Based on One Dimensional Nanostructured Metal-Oxides: A Review. *Sensors* **2012**, *12*, 7207–7258.
89. Andringa, A.-M.; Smits, E.C.P.; Klootwijk, J.H.; de Leeuw, D.M. Real-time NO2 detection at ppb level with ZnO field-effect transistors. *Sensors Actuators B Chem.* **2013**, *181*, 668–673.
90. Zeng, J.; Hu, M.; Wang, W.; Chen, H.; Qin, Y. NO2-sensing properties of porous WO3 gas sensor based on anodized sputtered tungsten thin film. *Sensors Actuators B Chem.* **2012**, *161*, 447–452.
91. Llobet, E.; Brezmes, J.; Ionescu, R.; Vilanova, X.; Al-Khalifa, S.; Gardner, J.W.; Bârsan, N.; Correig, X. Wavelet transform and fuzzy ARTMAP-based pattern recognition for fast gas identification using a micro-hotplate gas sensor. *Sensors Actuators B Chem.* **2002**, *83*, 238–244.